Heliyon 10 (2024) e25662

Contents lists available at ScienceDirect

Heliyon

journal homepage: www.cell.com/heliyon

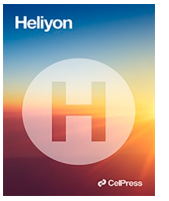

Research article

Drivers of tidal flow variability in the Pussur fluvial estuary: A numerical study by HEC-RAS

Motiur Rahman [a,b], Md. Shahjahan Ali [a,*]

[a] Department of Civil Engineering, Khulna University of Engineering and Technology, Khulna, 9203, Bangladesh
[b] Mongla Port Authority, Mongla, Bagerhat, Bangladesh

ARTICLE INFO

Keywords:
HEC-RAS
Hydrodynamics
Pussur river
Tidal flow
Tidal propagation

ABSTRACT

This paper aims at characterizing the longitudinal and temporal variability of tidal flows in the Gorai-Pussur River system of Bangladesh, which spans about 158 km, starting from Bordia upstream to Akram Point downstream. Considering the upstream fresh water discharge and the downstream tide level as the drivers of tidal flow variability, the spatiotemporal change in hydrodynamics of the Pussur Fluvial Estuary was simulated using HEC-RAS software at the neap-spring and seasonal scales. The model was calibrated by comparing the simulated discharge and water levels with available measured data at an intermediate station. During the dry season, the tidal effect from the sea reaches Bordia, while in the monsoon season, the tide reaches about 15 km less (up to Kalia) due to the increased flow of freshwater. The Pussur river experiences tidal amplification up to Chalna, located approximately 90 km from its mouth. Beyond Chalna, tidal dumping covers a distance of 100–170 km upto Bordia. The tidal range ratio between Akram Point and Mongla is 1.28. The phase shift of the high water is found approximately 1.0 h over a distance of 50 km. It is found that due to 50% increase of discharge in Bordia, the increase of discharges at Kalia and Chalna were found as 43% and 7%, respectively. For a 0.5 m increase in water level at downstream (Akram Point), the high and low water levels at Chalna are increased by 0.15 and 0.69 m, while for 1.0 m increase in water level at downstream, the high and low water levels at Chalna are increased by 0.67 and 1.20 m, respectively.

1. Introduction

The study of river hydrodynamics is a crucial aspect of comprehending the physical mechanisms that govern the movement of sediment in river systems. Tidal circulation frequently serves as the primary or principal secondary force that drives hydrodynamics. The propagation of astronomic tides into estuaries leads to the generation of high-frequency harmonics through nonlinear processes. Many researchers have developed hydrodynamic models of rivers and estuaries like the Amazon (Peru), Mississippi (Gulf of Mexico), Yangtze (China), Mekong River (Vietnam), Volta (Ghana), Purna (India), Damodar (India), etc. The Amazon River is the largest in the world and crosses eight countries on its pathway. Chávarri et al. [1] developed a 1-D hydrodynamic model of this river to simulate the geometry and flow field, which were not easily available in the Amazon context. The Yangtze River possesses one of the largest river basins globally and is ranked third in terms of runoff and drainage area. The flow regime within the middle Yangtze River Basin is currently undergoing significant transformations as a result of extensive human activities and the ongoing effects of climate change.

* Corresponding author.
E-mail address: msali@ce.kuet.ac.bd (Md.S. Ali).

https://doi.org/10.1016/j.heliyon.2024.e25662
Received 17 November 2023; Received in revised form 31 January 2024; Accepted 31 January 2024
Available online 7 February 2024

Lai et al. [2] simulated this system including the complex river-lake interactions. The freshwater flow of the Mississippi River has been altered significantly by dams, canalization, spillway openings, and diversions, which have been studied through hydrodynamic modeling [3]. The findings derived from the HEC-RAS hydraulic model of the Volta River in Ghana serve as a foundation for evaluating potential sedimentation issues in the Lower Volta River and for supporting the formulation of sediment control and management strategies for river basins in Ghana [4]. The flood vulnerability zones of the Purna and Damodar rivers in India were also identified through 1-D HEC-RAS hydrodynamic models [5,6]. The Mekong River Delta (MRD), covering 49,500 km^2, is the third largest delta plain in the world, trailing the Amazon and Ganges-Brahmaputra Deltas, and is home to the largest river in Southeast Asia [7]. The flat, low-lying terrain of MRD in Vietnam is characterized by a highly intricate network of rivers, channels, and flood plains. Le et al. [8] predicted the impact on the flooding in Vietnam's MRD of local man-made structures, sea level rise, and upstream flows through numerical modeling.

Bangladesh is a low-lying riverine country in South Asia, with a coastline of 710 km on the northern border of the Bay of Bengal, formed by a delta plain at the confluence of the Ganges (Padma), Brahmaputra (Jamuna), and Meghna Rivers and their tributaries [9]. The average annual surface water flow in Bangladesh is approximately 13,23,534 million cu.m., of which about 93% flows through the transboundary rivers from India and the rest 7% comes from rainfall [10]. The Padma (Ganges) is one of the major three rivers of Bangladesh that plays an important role in the hydrodynamics and morphological changes of other rivers [11–13]. Gorai River is one of the main tributaries of Padma, whose average flow is 1012 m^3/s or 31,915 million m^3/year, which is approximately 2.4% of the country's total annual flow. The downstream of Gorai has been named Nabaganga, Rupsha, and Pussur, which finally met with the Bay of Bengal in the south. Freshwater delivered by the Gorai River is bifurcated into the Pussur and Baleswar River systems via the Nabaganga and Madhumati at the Bordia area. Only around 15% of the water flows down the Baleswar River, while the Pussur River system handles roughly 85% of Gorai's flow [14]. The Pussur-Sibsa estuary is a complex network of river systems in the southwest region of Bangladesh. The river splits into the Sibsa River (west branch) and the Pussur River (east branch), about 30 km upstream from its mouth at Akram Point. The Sibsa River receives a very limited amount of freshwater flow because it's not connected with the upstream river properly. There are several small canals that connect the Pussur and Sibsa rivers.

Although tidal action dominates the flow of Pussur and Rupsha, the flow of Madhumoti is reliant on freshwater flow. According to Zaman et al. [15], a strong tide propagates about 160–170 km upstream of the coast. The Sibsa River is deeper than the Pussur, and hence the tidal wave propagates much faster in the Sibsa River than in the Pussur [16]. Previous studies reported that the scarcity of freshwater flow in the Pussur River system is one of the main reasons for its siltation problem [17,18]. The construction of Polders has reduced the tidal prism and silted up the peripheral channels, which has reduced the navigability of the rivers [19,20]. Cyclonic storm surge is one of the main reasons for flooding in the southwest region of Bangladesh [21,22]. Previous studies reported that the mean sea level is gradually rising at a rate of about 3 mm per year [19,23]. An increase in the tidal level of the Pussur River may affect the upstream area significantly [24]. This paper is aimed at studying the hydrodynamics of the above-mentioned river system.

Hydrodynamic models that replicate the hydraulic behavior of river channels have proven to be an effective instrument for floodplain management [25,26]. In the past, numerous researchers have studied the behavior of rivers and their flow phenomena on temporal and spatial scales through numerical modeling [27–30]. The study of surface water systems typically involves a combination of theoretical analysis, laboratory experiments, mathematical models, and field observations. However, for a complex body of surface water, reported or measured data are often insufficient to reflect or forecast the true condition. The present work provides a crucial reference for similar rivers in Bangladesh as well as other lower delta countries where the river flow is dominated both by tidal effects and upstream flow with a significant amount of seasonal variations.

Sometimes, researchers may get a skewed or inaccurate image of the situation if they rely on the available data, which isn't always reliable. Mathematical modeling in such instances requires observational verification and calibration. Complex water-related processes can be better understood, simulated, and predicted with the use of hydrodynamic models. The Hydrologic Engineering Centers-River Analysis System (HEC-RAS) is a good example of an integrated hydraulic and hydrologic modeling tool that can be used to generate hydrodynamic models with steady and unsteady flows.

HEC-RAS is a graphical user interface (GUI)-based, integrated suite of hydraulic analysis applications. Although 2D models give a two-dimensional presentation of the flow field, for a long reach of a channel, it is sometimes not practically feasible and efficient in terms of computational time and input requirements. Moreover, when it is required to carry out numerous numbers of test cases to study the flow phenomena for different scenarios (i.e., for different upstream and downstream boundary conditions or any other variations in input parameters), two-dimensional models become very time-consuming, especially if the flow domain is large. On the other hand, in field applications where an immediate response is required, a one-dimensional model can provide quick solutions. Therefore, the one-dimensional hydrodynamic model still draws attention from many researchers and practitioners. Horritt and Bates [31] evaluated the effectiveness and precision of three models of a 60-km segment of the Severn River in the United Kingdom. The tested models were HEC-RAS (1D), LISFLOOD-FP, and TELEMAC-2D. They discovered that the 1D HEC-RAS model was a better and more accurate predictor of flood flow rates than both of the 2D models when applied to the shape of their river using a DEM raster with enough detail to project the HEC-RAS results onto.

Mongla Port (MP), an important commercial hub in Bangladesh, is located on the east bank of the Pussur River. The hydrodynamics and morphology of the Pussur River are important for the economy of Bangladesh because of the presence of the sea port at its bank. To enhance the navigability of the Pussur River, several dredging projects have been implemented and will be required in the future [32]. Before the implementation of any capital dredging activities, numerical modeling is needed to be carried out to select the best-suited alignment. Besides the berths of MP, the industries on both sides of the Pussur River are constructing berths for their own or their clients' ships. Before the construction of any berth, it is necessary to conduct a hydrodynamic model to evaluate its effect on river morphology. However, the Pussur River only has two water level measurement stations and doesn't have any time-series discharge

data. Due to the absence of discharge data, researchers and modelers always face difficulties in developing any model of this river. This study used the Gorai River's discharge data (about 94 km upstream of Mongla) to generate the time series discharge of the Pussur River. Moreover, as far as the authors' knowledge is concerned, the temporal and spatial propagation of tide and its seasonal variations were not studied for this river, though it is an international navigation route.

In this study, considering the upstream fresh water discharge and the downstream tide level as the drivers of tidal flow variability, a one-dimensional HEC-RAS model was developed for the about 158 km-long Gorai-Pussur River system, where the upstream part covers about 94 km (from Bordia to Mongla) and the downstream part covers 79 km of length (from Chalna to Akram Point). In these two models, around 12 km have overlapped (Mongla to Chalna). It has been studied how the river's flow and tidal level change over time and space at the neap-spring and seasonal scales, along with the impact of fresh water flow upstream and raised tide levels downstream.

2. Study area and methodology

2.1. Study area

The study covers about 158 km of the Pussur River system from Bordia to Akram Point, as shown in Fig. 1. The Bordia station on the Gorai River is about 199 km downstream of the Gorai offtake point, where it is bifurcated into two streams, and Gorai-Pussur is the

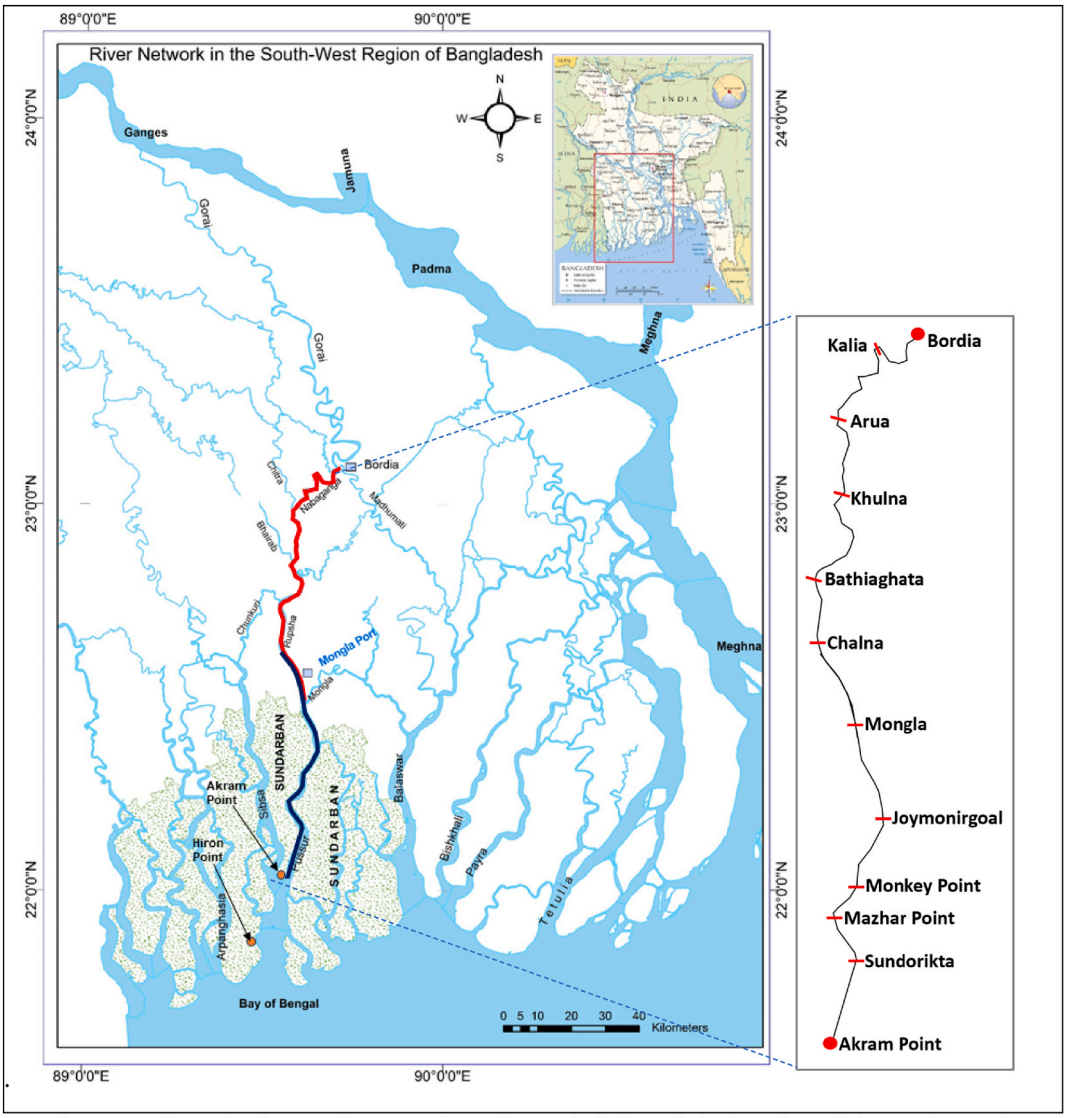

Fig. 1. Rivers in the southwest region of Bangladesh and the location of the study reach.

main branch of it that carries about 85% of Gorai's flow. Therefore, the southwestern part of Bangladesh receives freshwater from the Ganges through the Gorai-Pussur River system. Two mentionable rivers that meet with this river system are Chitra and Bhairab. However, these two rivers don't have freshwater flow sources upstream. Downstream, the tidal flow originated from the Bay of Bengal is divided among the Pussur and Sibsa rivers at Akram Point, and this tidal variation penetrates upstream up to Bordia Station. Mongla Port is located about 94 km downstream of Bordia and about 64 km upstream of Akram Point. For the convenience of model development, the study reach has been divided into two segments: Bordia to Mongla and Chalna to Akram Point.

2.2. Data

In this study, the bathymetric data for Akram Point to Chalna was collected from Mongla Port Authority (MPA), and that for Chalna to Bordia was collected from CEGIS (Center for Environmental and Geographic Information Services), Bangladesh. The hourly water level data for the January 2019 to December 2019 period for Akram Point and Mongla Point were collected from MPA, and the hourly discharge data for Bordia Point was collected from the Bangladesh Water Development Board (BWDB) for the period of January 2019 to December 2019. BWDB is a governmental agency tasked with the management of surface water and groundwater resources in Bangladesh. The data collected by BWDB is duly checked and verified before publication, which is reliable and acceptable to national and international researchers. Based on the collected bathymetry data, the longitudinal bed profile and channel width of the rivers are presented in Figs. 2 and 3. The topography of the river at Chalna to Bordia does not show any distinct meandering pattern. The channel is mostly shallow from Chalna to Mongla, where the depth is less than 5 m. However, in Chalna-Khulna, depth varies between 6 and 20 m, while it increases up to 27 m in some portions upstream of Khulna. After Arua, the depth reduced, and at Bordia, the depth was observed to be about 5.0 m (Fig. 2(a)). The width of the river in the studied stretch varies between 250 m and 1120 m. The width of the channel is more than 500 m up to Khulna, which has gradually decreased upstream (Fig. 2(b)).

The topography of the river at Chalna to Joymonirgol is approximately straight (Fig. 3(a)). After Joymonirgol, the river has a few sharp bends, where the depth is higher. The area from Mongla to Joymonirgol is also shallow, but in the downstream area from Joymonirgol to Akram point the depth varies between 8 and 24 m. The width of the river in the studied stretch varies between 700 m and 3500 m (Fig. 3(b)).The river segment between Joymonirgol to Akram Point is naturally deep and never required any dredging. But the upper part i.e. Chalna to Joymonirgol is crucial for navigation, and continuous maintenance dredging is required here.

2.3. Simulation techniques and test cases

The geometry of the model was developed using HEC-GeoRAS in ArcGIS. In this study, HEC-GeoRAS 10.2 in ArcGIS 10.2 has been

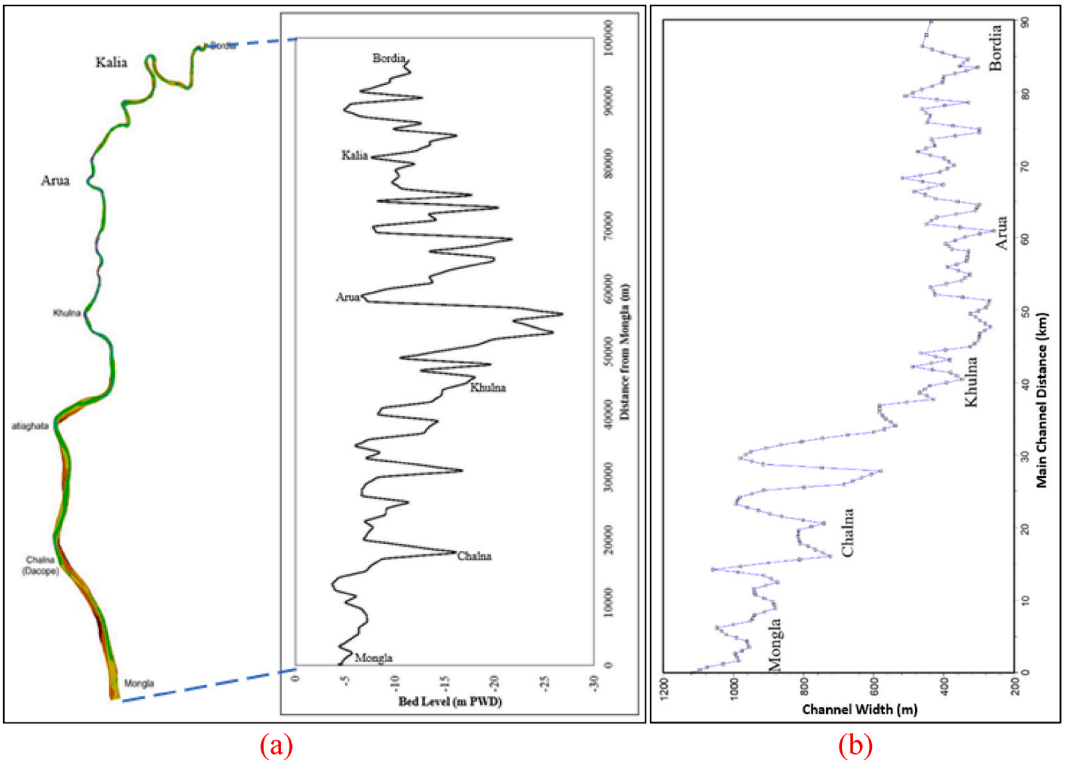

Fig. 2. Longitudinal Profile of channel from Bordia to Mongla (a) bed topography (b) channel width.

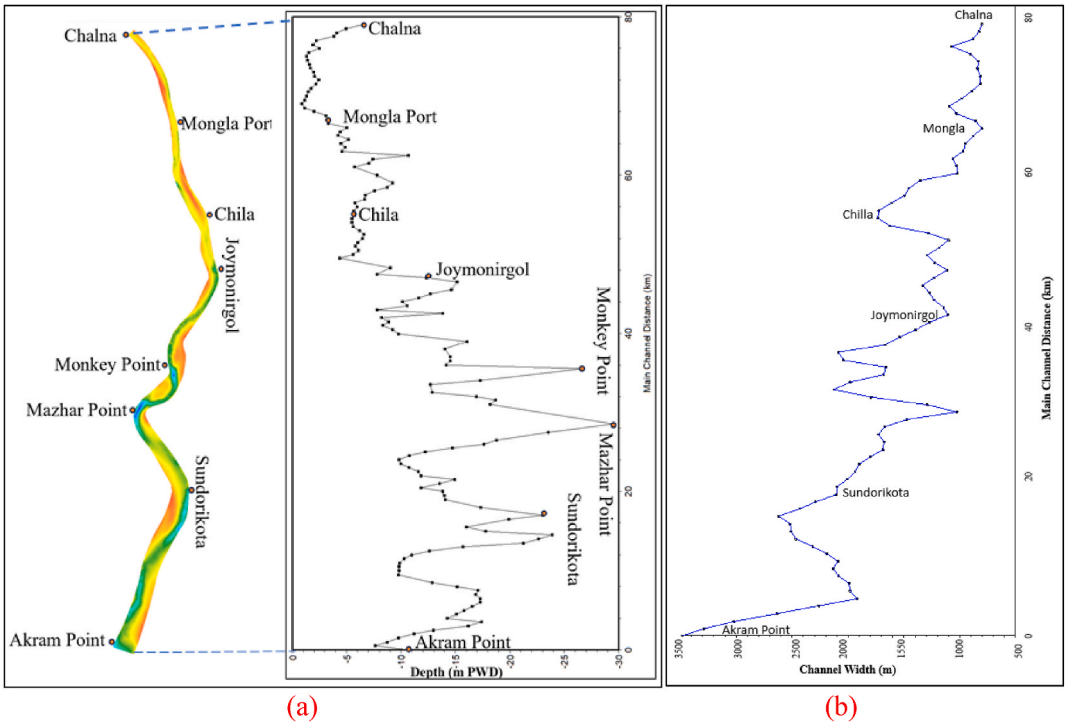

Fig. 3. Longitudinal profile of channel from Chalna to Akram point (a) bed topography (b) channel width.

used. HEC-RAS is a hydraulic model established by the U.S. Army Corps of Engineers Hydrologic Engineering Center (USACE HEC) to simulate river flow. It is a well-established and well-tested model that is used to evaluate the performance of other hydrodynamic modeling software. The initial version of the software, was developed in 1995 as a one-dimensional (1D) open-channel flow analysis tool. The current version offers users the ability to conduct 1D/2D unsteady flow modeling, sediment transport/mobile bed calculations, and water temperature/water quality modeling for a complete network of natural and constructed channels, or a single river segment, all within a user-friendly graphical user interface (GUI). For the 1D unsteady flow computation, HEC-RAS solves the full 1D Saint-Venant equation using an implicit finite difference method. The energy and momentum equations are utilized to derive the 1D Saint Venant equations when solving steady and unsteady flows within HEC-RAS using the implicit finite difference approach. The basic equations used in HEC-RAS simulation are given below:

$$\frac{\partial A}{\partial t}+\frac{\partial Q}{\partial x}=0 \tag{1}$$

$$\frac{\partial Q}{\partial t}+\frac{\partial\left(\frac{Q^3}{A}\right)}{\partial x}+gA\frac{\partial H}{\partial x}+gA\left(S_0-S_f\right)=0 \tag{2}$$

where A represents cross-sectional area; t is time, Q is water flow; x is the measured distance in the direction of the channel; g is the gravitational acceleration; H is the height of water level above the datum; S_o is the slope of the river bed and S_f is the energy slope.

As stated earlier, the model was developed in two parts, in Model-1, the Chainage is defined as 0 at downstream (Mongla) and 94,000 m at upstream (Bordia). In Model-2, the Chainage at downstream (Akram point) is 8500 m and at upstream (Chalna) is 87,000 m. The simulation period of Bordia to Mongla was 01/01/2019–31/12/2019. The Model-1 covers some parts of the Pussur River, Rupsha River and Nabaganga River, whose bathymetry was collected from a secondary source (CEGIS). The point bathymetry data was converted to Raster and then to TIN in ArcGIS. Using the TIN, the river geometry was prepared at 1000 m intervals which was interpolated at 500 m intervals in HEC-RAS (Fig. 4).

In the Model-1, the hourly discharge data at Bordia Point of Gorai River was used as the upstream boundary condition, and the hourly water level data at Mongla was used as the downstream boundary. The discharge measuring point of BWDB is a few km upstream of Bordia. According to previous research [16], 85% of the flow of Gorai is diverted to the Pussur River system at Bordia. Based on that, 85% hourly discharge data of Gorai River at Bordia was used as the upstream boundary condition.

The simulated discharge at Chalna from Model-1 is used as upstream boundary condition of the Model-2 and the flow field is calculated for the year of 2019. In the Model-2, the hourly water level data at Akram Point collected from MPA was used as the downstream boundary. Table 1(a) shows the details of two methods, which are denoted as base cases. For Model-1 (Case C1R1), the simulated results are calibrated and validated comparing the discharge and water level data at Chalna, respectively. For Model-2 (Case

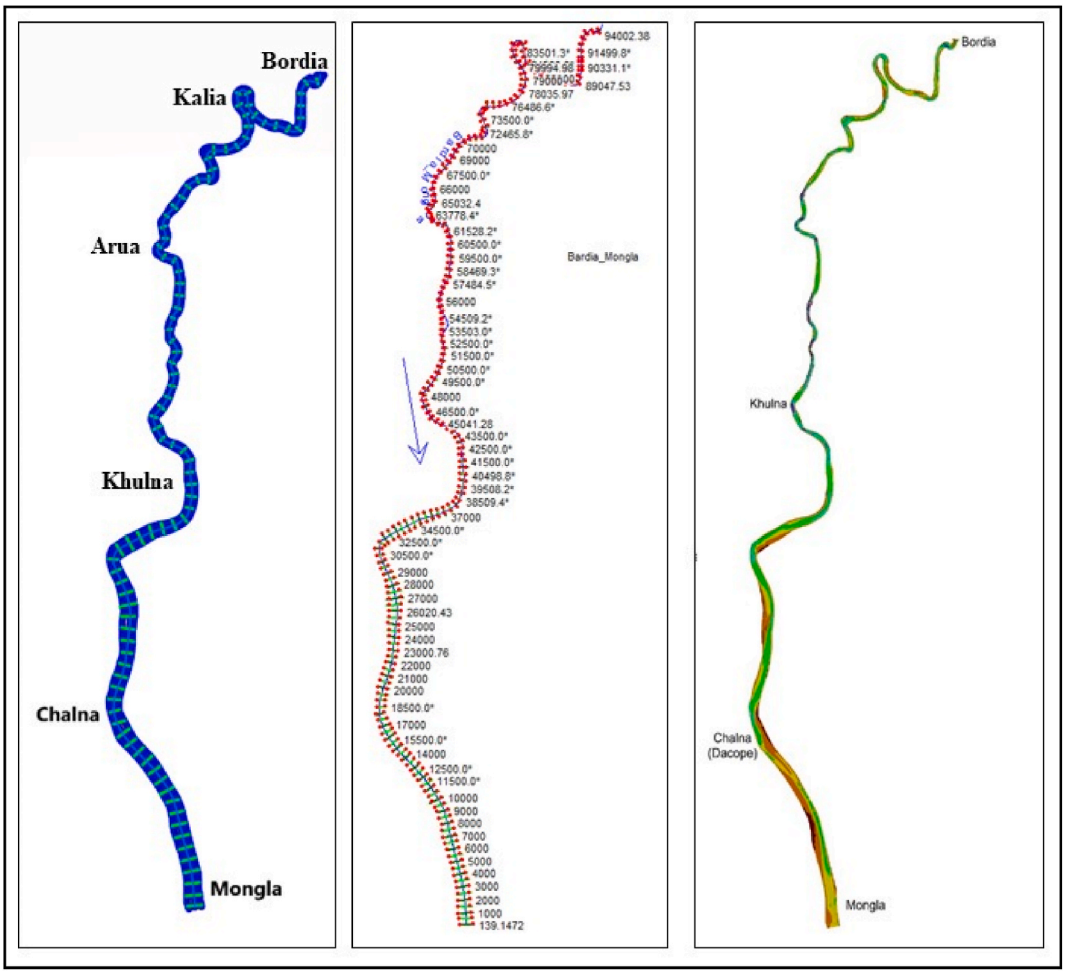

Fig. 4. Geometry and bathymetry of Model-1.

C2R1), the water level at Mongla was used for calibration. Upstream discharge and downstream tidal water level are considered here as the driver for tidal flow variations. In this study, the effect of upstream freshwater flow was evaluated comparing the simulated results for various discharges. The upstream discharge was increased by 10%, 30% and 50% for cases C1R2, C1R3 and C1R4 (as shown in Table 1(b)), respectively and the results are compared with base case C1R1. Similarly, the downstream water level was increased by 0.5 m and 1.0 m (Case C2R2 and C2R3, respectively), and the simulated results are compared with base case C2R1 to assess the effect of downstream water level on simulated flow field.

2.4. Calibration and validation of model

The model of Bordia to Mongla (Model-1) was calibrated and validated using the observed discharge and water level data for Chalna station, respectively (Figs. 5(a) and 6(a)). The comparison shows a correlation coefficient of 0.935 for discharge and 0.868 for water level as shown in Figs. 5(b) and 6(b), respectively. From the output data of the calibrated model, the hourly discharge data at Chalna was extracted to use as the upstream boundary of Model-2. The hourly water level data at Hiron Point was collected for the

Table 1(a)
Simulation conditions for two models.

Cases	Study reach	Upstream Boundary Condition	Downstream Boundary Condition	Station for Calibration/ Validation
Model-1 (Case C1R1)	Mongla-Bordia (94.0 km)	Time series discharge for one year at Bordia	Time series Water Level for one year at Mongla	Discharge and water level at Chalna
Model-2 (Case C2R1)	Akram Point -Chalna (79.5 km)	Time series discharge for one year at Chalna	Time series Water Level for one year at Akram Point	Water level at Mongla

Table 1(b)
Description of simulation cases.

Case Notation	Description	Case Notation	Description
C1R1	Base Case (Model 1)	C2R1	Base case (Model 2)
C1R2	Discharge at upstream boundary (Bordia) increased by 10%	C2R2	The water level at downstream boundary (Akram Point) increased by 0.5 m
C1R3	Discharge at upstream boundary (Bordia) increased by 30%	C2R3	The water level at downstream boundary (Akram Point) increased by 1 m
C1R4	Discharge at upstream boundary (Bordia) increased by 50%	–	–

study period. As per MPA, the time shifting required to get the water level at Akram Point is 1 h later than at Hiron Point.

The water level data of the Hiron point has been used as the downstream boundary of Model-2 applying the time shifting. This model was calibrated at Mongla using the measured water level as shown in Fig. 7(a). It is to be mentioned that, all the bathymetry was in the mPWD datum, and MPA measured the water level with respect to Chart Datum (CD). Before applying the water level data in the model, it was converted to mPWD. The comparison shows a correlation coefficient of 0.988 for water level as shown in Fig. 7(b).

3. Result and discussion

After the development of the model, the detailed hydrodynamic features in all cases have been analyzed. For the analysis, July 02, 2019 was selected as the sample date of High Flow Season (HFS) and March 03, 2019 as Low Flow Season (LFS) of Model-1. In Model-2, 14/07/19 was considered as the sample date of HFS and 18/02/19 as LFS. The results of the two models are discussed separately in the following sections.

3.1. Simulation results for Bordia to Mongla (model-1)

The hydrodynamics of the river from Bordia to Mongla was simulated and the water level, discharge, velocity, tidal propagation etc. have been investigated at several locations of the study reach for the year of 2019 at neap-spring and seasonal scales. The outcomes of the hydrodynamic modeling are explained below.

3.1.1. General features of the simulated flow field

The water surface profile during high tide and low tide at Mongla is presented in Fig. 8(a) and (b) for LFS, and in Fig. 9(a) and (b) for HFS, respectively. These figures show the variation of tides along the longitudinal direction. On LFS, the high tide at Mongla was at 12:00 h and at that time low tide was observed in Kalia. Similarly, during low tide at Mongla, high tide was observed at Kalia. The difference in water surface at Mongla and Kalia is about 1.5 m in LFS. On July 2, 2019 (HFS), the high tide at Mongla was at 11:00 h and at that time low tide was observed in Kalia. During low tide at Mongla, high tide was observed at Kalia. The difference in water surface at Mongla and Kalia is about 2.5 m in HFS.

The velocity in the longitudinal direction is also found to be varied in flood tide and ebb tide. According to the model result, the velocity in LFS at Mongla was 1.2 m/s and 0.65 m/s during flood tide and ebb tide, respectively. But, in HFS the velocity was 0.95 m/s and 1.7 m/s during flood tide and ebb tide, respectively. In Mongla, the velocity of flood tide is higher than ebb tide in the LFS, which is reversed in the HFS. Velocity difference between high and low tide is higher in the HFS than LFS. The velocity variations during high tide compared to low tide in LFS and HFS are presented in Fig. 10(a) and (b), respectively. The velocity of Mongla during the HFS in

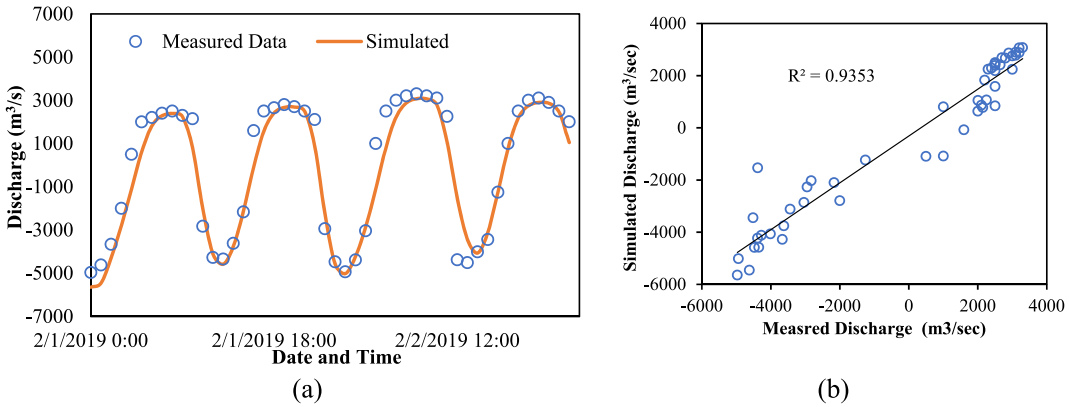

Fig. 5. Comparison of simulated discharge with available measured data at Chalna station (a) Tidal variation of discharge (b) Correlation coefficient.

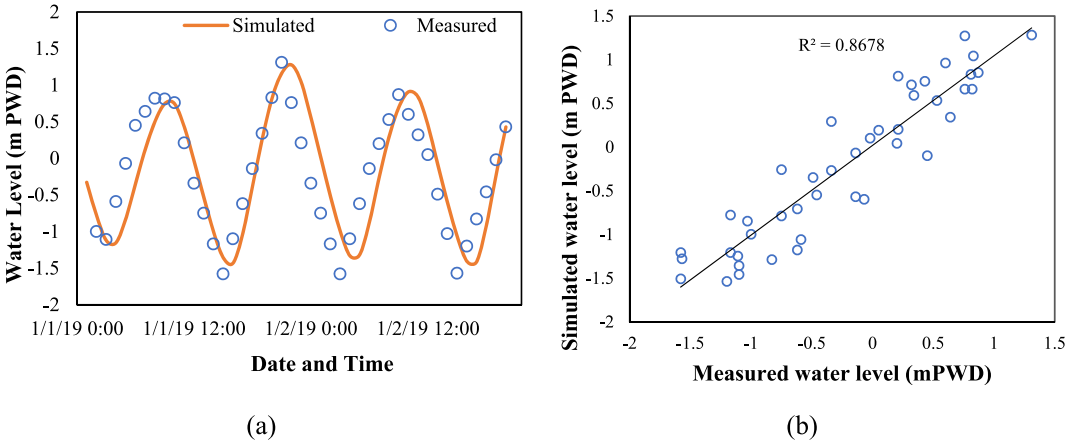

Fig. 6. Comparison of simulated water level with available measured data at Chalna station for Model-1 (a) Tidal variation of water level (b) Correlation coefficient.

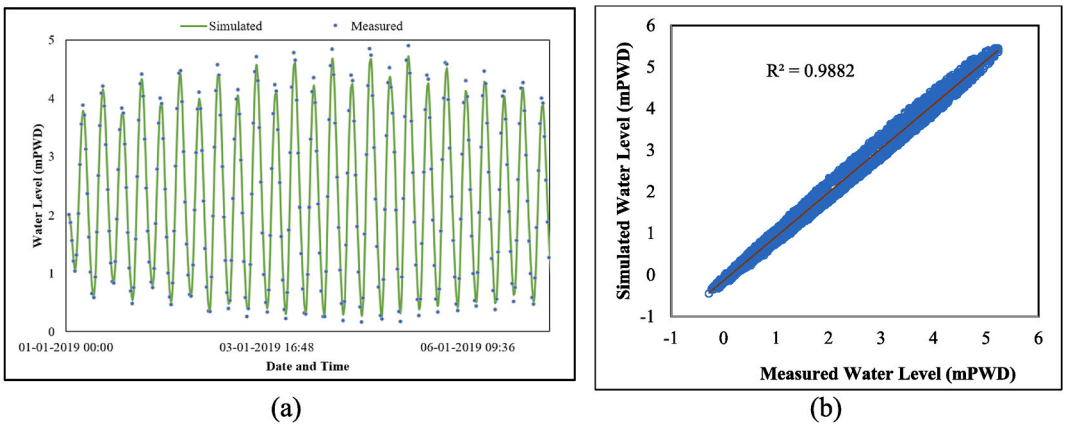

Fig. 7. Comparison of simulated water level with available measured data at Mongla station for Model-2 (a) Tidal variation of water level (b) Correlation coefficient.

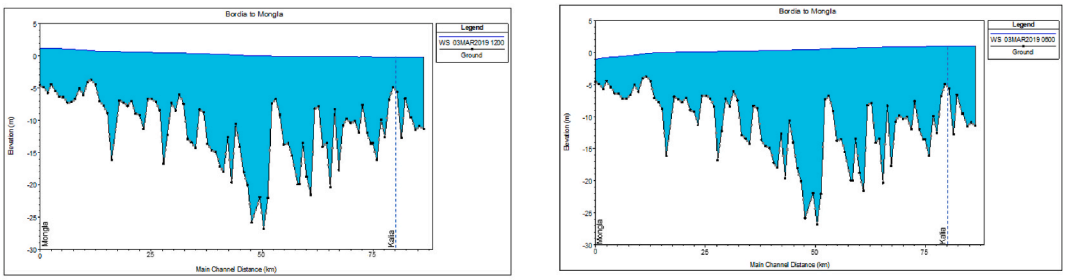

Fig. 8. (a): Water surface profile during high tide at Mongla in LFS.
(b): Water surface profile during low tide at Mongla in LFS.

high tide is higher than the LFS; however, at Khulna and its upstream, the same velocity is lower during the HFS than the LFS. In low tide, the velocity during LFS is lower everywhere than the HFS. This variation is presented in Fig. 11(a) and (b).

The tidal phase of discharge and corresponding water level is presented in Fig. 12. It is observed that they are in reverse order. From the simulated data, it is found that in 2019, the maximum flow at Chalna during the dry season (November–March) was 3973 m^3/s,

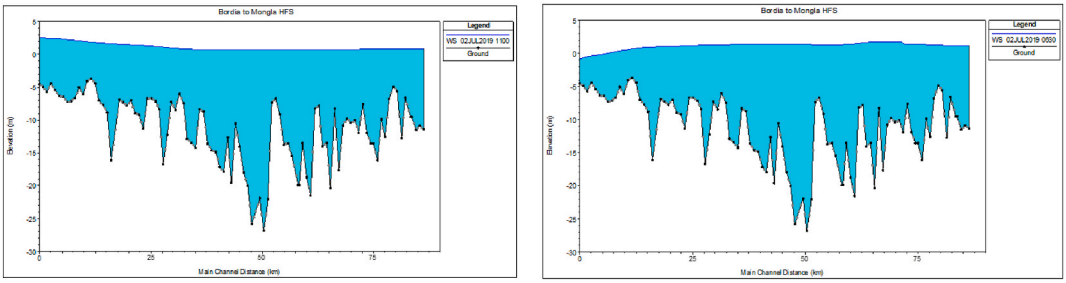

(a): Water surface profile during high tide at Mongla in HFS.

(b): Water surface profile during low tide at Mongla in HFS.

Fig. 9. (a): Water surface profile during high tide at Mongla in HFS.
(b): Water surface profile during low tide at Mongla in HFS.

and in the monsoon season (June–October) 4145 m^3/s. The seasonal variation in maximum discharge is about 5% only. However, at the upstream boundary during the dry season the maximum flow was 18 m^3/s, and in the monsoon season it is 4206 m^3/s. It implies that the flow at Chalna is dominated by tidal flow rather than upstream flow.

The magnitude of flow reduces gradually towards upstream in both seasons as presented in Fig. 13(a) and (b). In both the seasons, the flow in flood tide is higher than ebb tide. The flood flow is 15% higher than the ebb flow in the LFS and 41% higher in the HFS. The flow in the HFS is increased by 93% in flood tide and 58% in ebb tide.

3.1.2. Tidal propagation

The Mean Monthly Flow (MMF) of Gorai River is 262% higher in the high flow season (HFS) than in the low flow season (LFS) [33]. Therefore, it is expected that, at least in HFS, the freshwater flow at Bordia may affect the tidal propagation at its downstream. Location wise variation of flow in monsoon and dry season is presented in Fig. 14. In dry season, tidal effect of flow was observed upto Kalia (Fig. 14(a)). However, in monsoon, the discharges are found to be constant with time and no tidal variation was observed in Kalia (Fig. 14(b)). The water level at 5000 m intervals has been analyzed to determine the face of the tide and the time required to reach different locations. The variations of water level with time at different locations are presented in Fig. 15(a) and (b) for HFS and LFS, respectively. It is observed that on July 02, 2019 (HFS) the high tide at Mongla was at 11:00 h. The front of high tide takes about 1.45 h to reach Chalna and 3 h to reach Khulna. Up to Kalia the tides dominate the flow, and after that its effect is negligible. During LFS, the high tide at Mongla was at 12.00 h. The face of high tide takes about 1.1 h to reach Chalna and 2.5 h to reach Khulna. In this season the tide dominates up to Bordia. The tidal rise is lower at Khulna than in other areas. The propagation speed of tide in the HFS and LFS is presented in Table 2. Propagation speed is higher at Mongla to Khulna area than Khulna to Kalia; in Kalia to Bordia, the tidal effect is not noticeable.

Tide takes about 6.7 h to reach Kalia from Mongla in the HFS and 6.0 h in LFS. During LFS, since the upstream flow is very low, the tidal flow penetrates more and the tidal effect was observed up to Bordia.

3.1.3. Effect of upstream discharge

The effect of increased flow at Bordia on the downstream discharge has been evaluated by varying the flow at the upstream boundary. The flow has been varied up to 150% at Bordia in both seasons. It is observed that since the flow in LFS is very small compared to tidal discharge, in this season the increase of upstream flow does not have any significant impact on the tidal flow of the river. However, in HFS the increased upstream flow substantially impacts upto Kalia and the impact gradually decreases towards

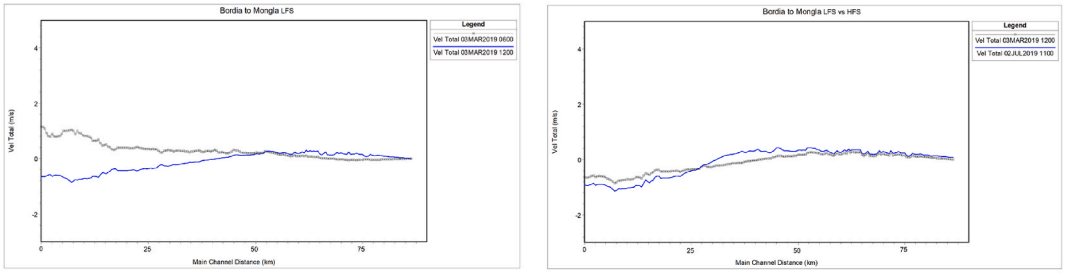

(a): Velocity variation in high tide compared to low tide in LFS.

(b): Velocity variation in high tide compared to low tide in HFS.

Fig. 10. (a): Velocity variation in high tide compared to low tide in LFS.
(b): Velocity variation in high tide compared to low tide in HFS.

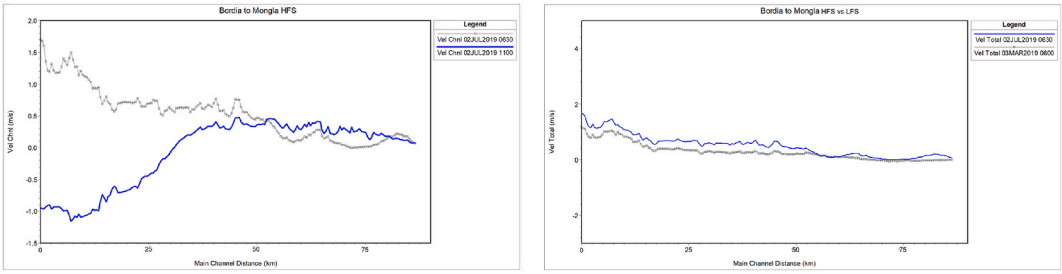

(a): Comparison of longitudinal velocity for LFS with HFS in high tide case.

(b): Comparison of longitudinal velocity for LFS with HFS in low tide case.

Fig. 11. (a): Comparison of longitudinal velocity for LFS with HFS in high tide case.
(b): Comparison of longitudinal velocity for LFS with HFS in low tide case.

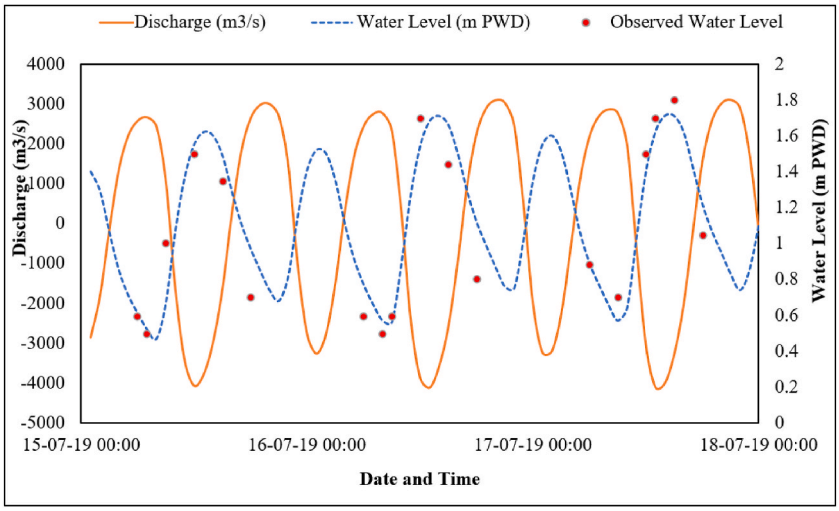

Fig. 12. Flow and water level at Chalna on 15–18 July 2019.

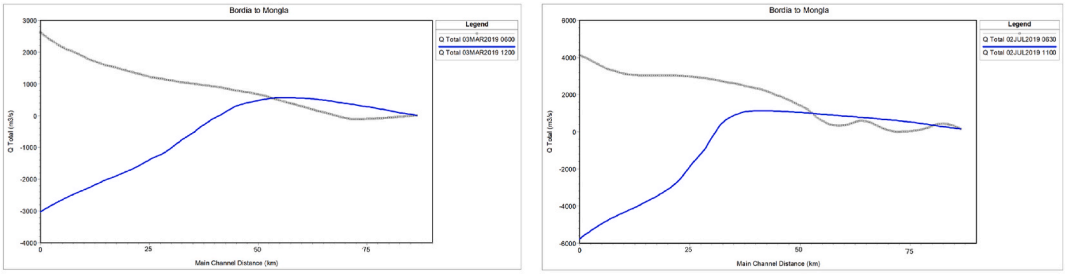

(a): Flow variation in flood tide and ebb tide in LFS.

(b): Flow variation in flood tide and ebb tide in HFS.

Fig. 13. (a): Flow variation in flood tide and ebb tide in LFS.
(b): Flow variation in flood tide and ebb tide in HFS.

downstream. Due to 50% increase of discharge in Bordia, the increase of discharges at Kalia, Chalna and Mongla are found as 43%, 7% and 2%, respectively.

3.2. Simulation results for Chalna to Akram point (model-2)

The hydrodynamics of the river from Chalna to Akram point was simulated and the water level, discharge, velocity, tidal

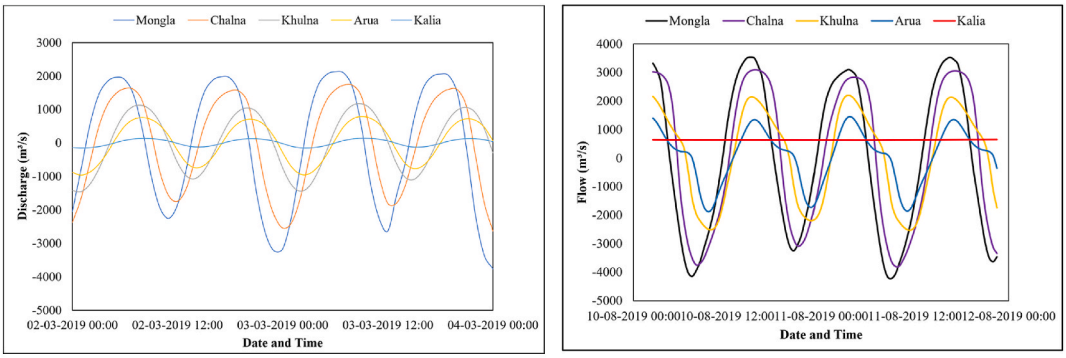

Fig. 14. (a): Flow variation at different location in dry season.
(b): Flow variation at different location in monsoon season.

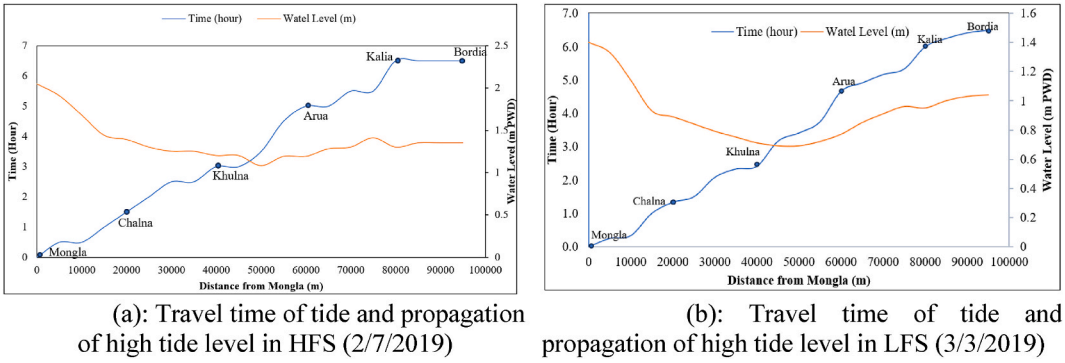

Fig. 15. (a): Travel time of tide and propagation of high tide level in HFS (July 2, 2019)
(b): Travel time of tide and propagation of high tide level in LFS (March 3, 2019).

Table 2
Propagation speed of tide.

From	To	Distance (m)	HFS		LFS	
			Time Req. (Min)	Tide Propagation Speed (m/min)	Time Req. (Min)	Tide Propagation Speed (m/min)
Mongla	Chalna	20,000	85	230	65	303
Chalna	Khulna	20,000	95	215	85	238
Khulna	Kalia	40,000	220	182	210	190

propagation etc. have been investigated at several locations of the study reach for the year of 2019. The date 14/07/19 was considered as the sample date of HFS and 18/02/19 as LFS. The outcomes of the hydrodynamic modeling are explained below.

3.2.1. General features of simulated flow

Longitudinal variation of water level at different locations has been analyzed for high tide and low tide periods in HFS and LFS, which is presented in Fig. 16. During the HFS, the high water level was found 2.4 mPWD at Chalna and 1.63 mPWD at Akram Point on high tide, and −1.35 mPWD and −0.95 mPWD on low tide.

In this season, the difference between Chalna and Akram points was 0.77 m on high tide and 0.40 m on low tide. During HFS, the differences between the high tide level and low tide level are 3.75 m at Chalna and 2.58 m at Akram Point.

During the LFS, the water level was found 1.69 mPWD at Chalna and 0.88 mPWD at Akram Point on high tide and −2.22 mPWD and −1.7 mPWD on low tide. In this season, the difference between Chalna and Akram points was 0.81 m on high tide and 0.52 m on low tide. During LFS, the difference between the high tide level and low tide level is 3.91 m at Chalna and 2.58 at Akram Point.

The high-water level and low water level at selected locations of Pussur River in the HFS and LFS are presented in Fig. 17(a) and (b), respectively. The differences in water levels are presented in Table 3. During the LFS, the high-water level is decreased by 0.71 m at Chalna and 0.75 m at Akram Point compared to HFS.

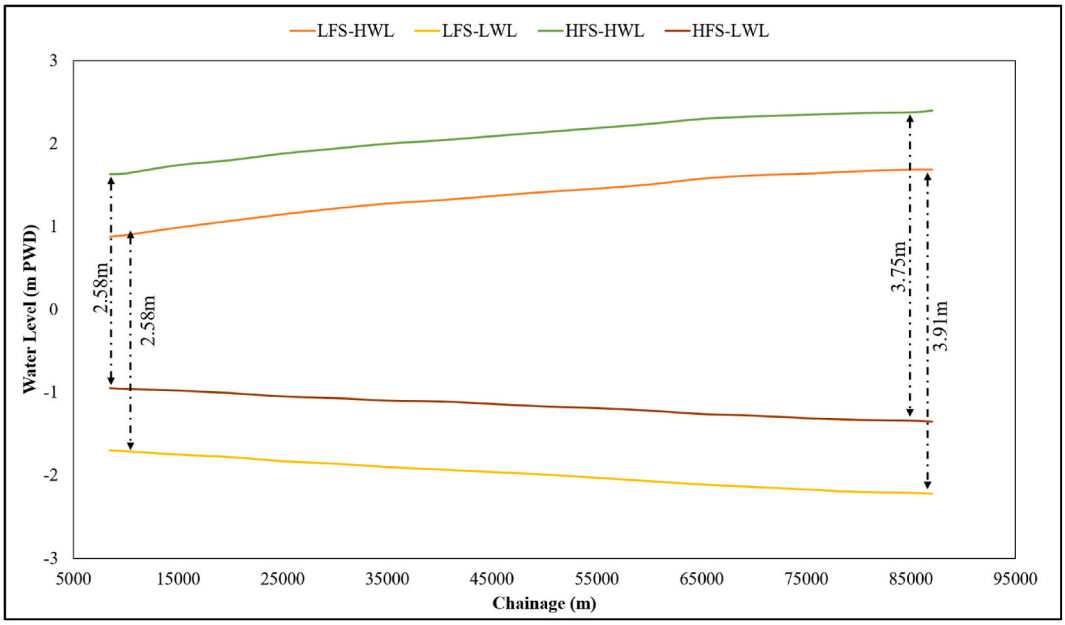

Fig. 16. Water level during high tide and low tide in LFS and HFS.

The comparison of velocity at high tide and low tide in both the HFS and LFS is presented in Figs. 18 and 19. In the HFS, the average velocity at Akram point is −0.9 m/s in high tide and 0.6 m/s in low tide, whereas at Chalna it is varied between 0.5 m and −0.5 m/s in both high and low tide. In this season the magnitude of velocity is almost the same in high tide and low tide at Chalna, but about 50% higher in high tide at Akram Point.

In the LFS, the average velocity at Akram point is −0.44 m/s in high tide and 0.36 m/s in low tide, whereas at Chalna it is −0.32 m/s in high tide and 0.48 m/s in low tide. In high tide, velocity is higher at Akram point than low tide, but at Chalna low tide velocity is higher than high tide.

Discharge of Chalna, Mongla, and Akram points has been analyzed during high tide and low tide at HFS and LFS. Comparisons of both the seasonal flows are presented in Figs. 20 and 21. In the HFS, maximum discharge was - 25,971 m^3/s at Akram point and - 4080 m^3/s at Chalna in high tide. During low tide, discharge is reduced to 16,652 m^3/s at Akram point and 3309 m^3/s at Chalna.

In the LFS, maximum discharge was - 14,173 m^3/s at Akram point and - 2837 m^3/s at Chalna in high tide. During low tide, the discharge reduced to 8776 m^3/s at Akram Point and 1784 m^3/s at Chalna. The seasonal reduction of flow is 45% and 32% in high tide and 47% and 45% in low tide at Akram Point and Chalna, respectively. Flow variation at Akram Point, Joymonirgol, Mongla, and Chalna in high tide and low tide during the HFS and LFS is presented in Table 4.

3.2.2. Tidal propagation

The stage hydrograph on HFS at Akram Point, Joymonirgol, Mongla, and Chalna is presented in Fig. 22. The phase difference of the hydrographs indicate the propagation of the tide. Fig. 23(a) and (b) represent the travel time of tide and corresponding water level

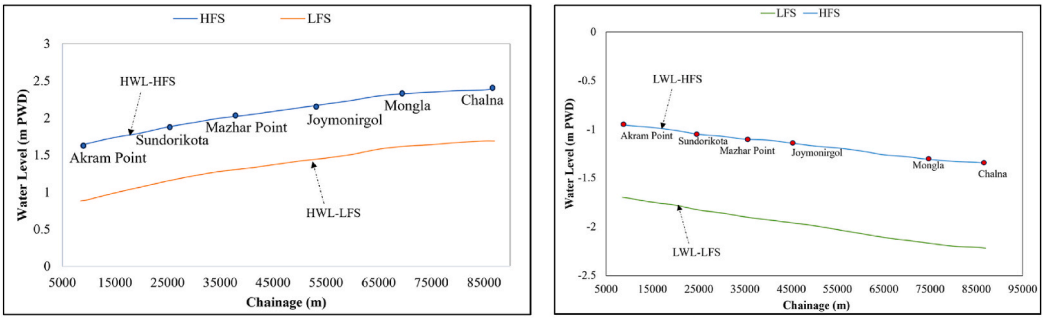

(a): Differences of HWL between HFS and LFS

(b): Differences of LWL between HFS and LFS

Fig. 17. (a): Differences of HWL between HFS and LFS.
(b): Differences of LWL between HFS and LFS.

Table 3
Water level difference in HFS and LFS.

Location	HWL (m PWD)			LWL (m PWD)		
	HFS	LFS	Difference (m)	HFS	LFS	Difference (m)
Akram Point	1.63	0.88	0.75	−0.95	−1.7	0.75
Sundorikota	1.88	1.15	0.73	−1.05	−1.83	0.78
Mazhar Point	2	1.28	0.72	−1.1	−1.9	0.80
Joymonirgol	2.09	1.37	0.72	−1.14	−1.96	0.82
Mongla	2.35	1.64	0.71	−1.31	−2.17	0.86
Chalna	2.4	1.69	0.71	−1.35	−2.22	0.87

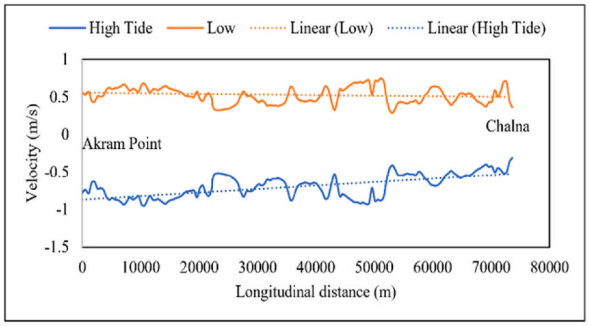

Fig. 18. Velocity comparison in HFS.

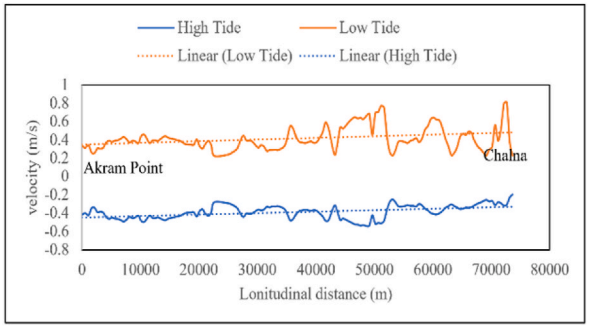

Fig. 19. Velocity comparison in LFS

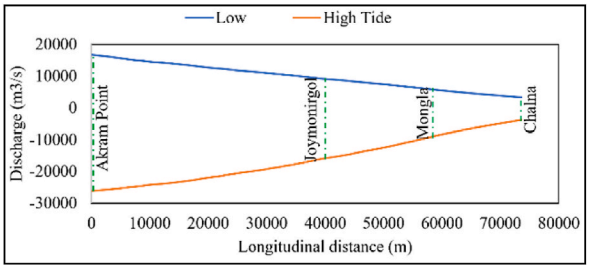

Fig. 20. Comparison of flow in HFS.

along the longitudinal distance for HFS and LFS, respectively. The model data shows that the tide from Akram Point takes about 55 min, 85 min, and 115 min to reach Joymonirgol, Mongla and Chalna, respectively. According to van Maren et al. [19], the travel time to Chalna is 115 min, which is similar to this model result. The tide propagation speed is found higher up to Joymonirgol because the depth in this segment is higher than in other areas. Moreover, the tide propagation speed is found higher in HFS than LFS.

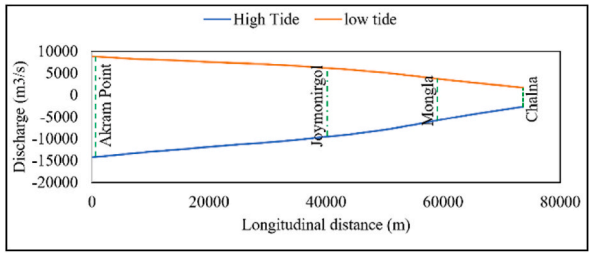

Fig. 21. Comparison of flow in LFS.

Table 4
Flow comparison in HFS and LFS.

Location	Discharge in HFS (m^3/s)		Discharge in LFS (m^3/s)	
	High tide	Low tide	High tide	Low tide
Akram Point	−25971	16,652	−14173	8776
Joymonirgol	−15735	9003	−9600	6131
Mongla	−8467	5361	−5760	3341
Chalna	−4080	3309	−2837	1784

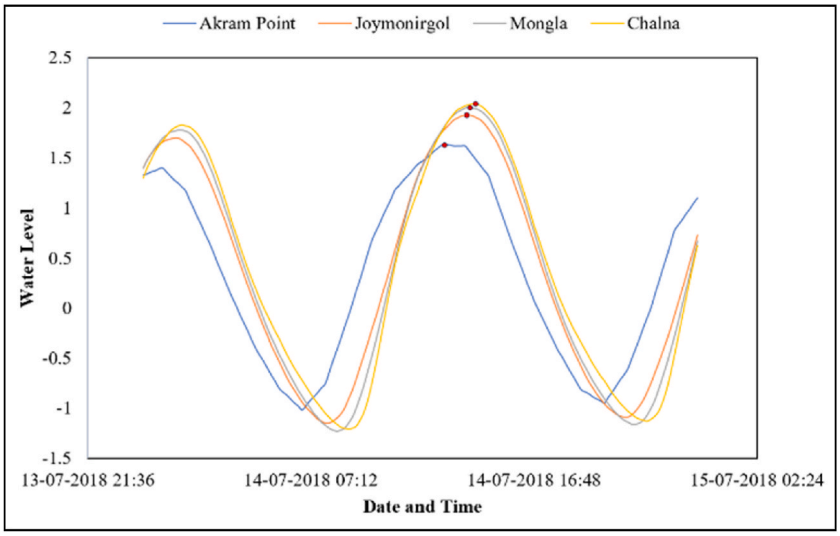

Fig. 22. Stage hydrograph on HFS.

3.2.3. Effect of downstream water level

The global trend of sea level rise has a multitude of effects on Bangladesh. Bangladesh has already experienced adverse consequences, including flood, cyclone, soil degradation, salinity intrusion, and biodiversity depletion. The potential hazards associated with this phenomenon are projected to intensify in the future [10]. The intensity and frequency of cyclone has already been increased in this region and causes frequent tidal surge that raises the water level at the estuary [34]. In future, the rise in sea level is anticipated to result in several adverse effects along the coast. The elevation of the Sundarban is ranged from about 0.44 to 1.35 mPWD [14]. The potential consequences of 1-m sea level rise (SLR) include significant impacts on the extensive coastal territory and floodplain zone of the country. To determine the effect of downstream water level on the upstream flows, in this study, two simulations were carried out by increasing the downstream water level at Akram point by 0.5 m and 1 m (Case C2R2 and C2R3, respectively), and the hydrodynamic consequences at upstream (at Chalna) have been analyzed comparing with base case C2R1.

Fig. 24 shows the high-water level variations at Chalna due to 0.5 m and 1.0 m increase in water level at Akram point for high and low flow seasons. Fig. 25 shows the same for low water level case. In both the figures, the blue color shows the water level at Akram point that found to be increased at upstream (Chalna). The increased amounts are shown in orange color. It is seen that the high-water levels at HFS at Akram point are 1.63, 2.13 and 2.63 mPWD for C2R1, C2R2 and C2R3 cases respectively, which are found as 2.4, 2.52 and 3.06 mPWD at Chalna. Similarly, the low water levels at LFS at Akram point are −1.70, −1.2 and −0.70 mPWD, which are lowered

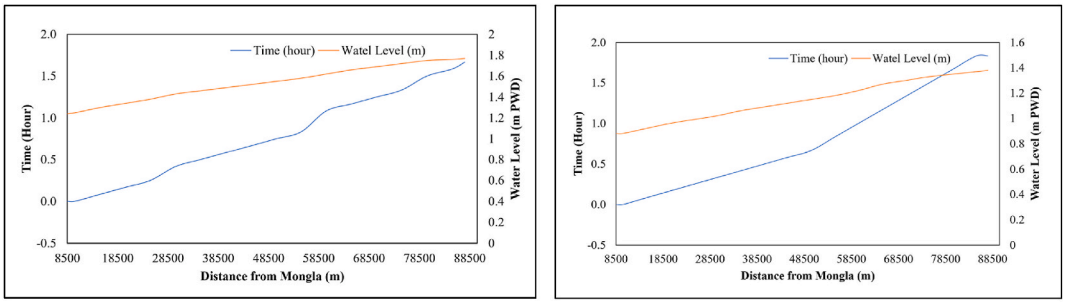

Fig. 23. (a): Travel time of tide and water level in HFS.
(b): Travel time of tide and water level in LFS.

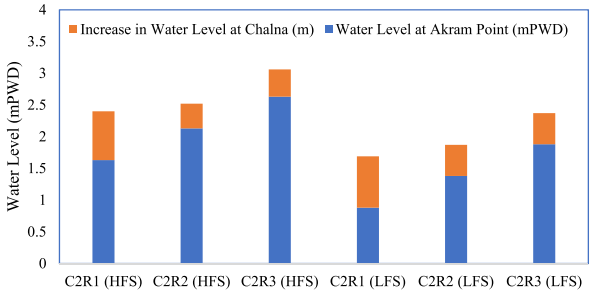

Fig. 24. High water level at Akram point and Chalna in high and low flow seasons for three cases (C2R1 is the base case, C2R2 and C2R3 are with 0.5 m and 1.0 m increased water level at Akram point).

to −2.2, −1.52 and −1.03 mPWD at Chalna for C2R1, C2R2 and C2R3 cases, respectively. The results are summarizing in Table 5. It is seen that for 0.5 m increase of water level at Akram point, the water level at chalna was found to be increased by 0.12 m in HFS and 0.18 m in LFS compared to base case (C2R1), which are 0.66 m and 0.68 m for 1.0 m increase of water level at downstream boundary. The effect of downstream water level was found more significant in the case of low water level. In low water level, for the 0.5 m increase of water level at Akram point, the water level at Chalna was found to be increased by 0.67 m in HFS and 0.70 m in LFS compared to base case (C2R1), which are 1.20 m and 1.19 m for 1.0 m increase of water level at downstream boundary. Increase of water level during low tide is higher than high tide in both cases. During the high tide, the increase at downstream water level affects the upstream less due to the fresh water flow from opposite direction. However, during low tide, the tidal flow and fresh water flow coincides in the same direction that affects the downstream significantly.

4. Discussion

The main purpose of this study is to see the effect of fresh water flow from Gorai river on its downstream as well as the propagation

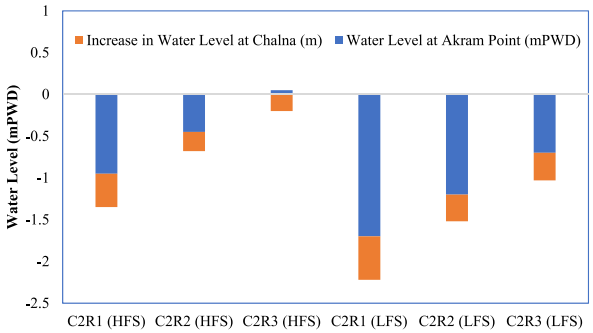

Fig. 25. Low water level at Akram point and Chalna in high and low flow seasons for three cases (C2R1 is the base case, C2R2 and C2R3 are with 0.5 m and 1.0 m increased water level at Akram point).

Table 5
Change in upstream flow (at Chalna) due to increase in Water level at downstream (Akram point).

Water Level increased at Akram Point (m)	Water Level increase at Chalna (m)			
	High Water Level		Low Water Level	
	HFS	LFS	HFS	LFS
0.5	0.12	0.18	0.67	0.7
1.0	0.66	0.68	1.2	1.19

of tidal effects from the sea on several sections of the river system. It is observed that the tidal effect from the sea propagates upto Bordia in dry season, whereas the tide propagates about 15 km less (upto Kalia) in monsoon season because of increased freshwater flow. Tide takes around 115 min to reach at Chalna from Akram Point and 315 min to reach at Kalia from Chalna. Propagation speed upto Chalna is faster than further upstream because of higher depth in downstream area. It is observed that the effect of increased freshwater flow at Bordia (up to 150% of present discharge) doesn't have significant effect on the hydrodynamics of the Pussur River at downstream of Chalna. This study assessed the effect of downstream water level on upstream flows. The results showed that for 0.5 m increase of water level at Akram point, the water level at Chalna was found to be increased by 0.12 m in HFS and 0.18 m in LFS compared to the base case. The effect of downstream water level was found more significant in the case of low water level. The increase of water level during low tide is higher than high tide in both cases. During high tide period the downstream impact is relatively reduced on the upstream due to the counter-directional flow of fresh water. However, during low tide period, the direction of tidal flow aligns with the direction of fresh water flow, resulting in a greater downstream impact.

Prandle [35] studied a set of 50 estuaries in UK and USA and found that the lengths of the estuaries were varied between 2 and 200 km and depths of 1–20 m. Van Rijn [36] studied the Western Scheldt Estuary in the Netherlands, the Hooghly Estuary in India and the Delaware Estuary in the USA. He reported that the length of funnel-shaped, synchronous, alluvial estuaries will be in the range of 5–400 km and in most of the estuaries the maximum velocity at the mouth is in the order of 1 m/s. The ratio of wave height to water depth is ranged about 0.1–0.4 in the mouth of most estuaries. The Pussur estuary has a length of about 200 km, where the depth varies from 4 to 30 m. The maximum velocity at the mouth is observed as near about 1 m/s (Figs. 18 and 19). The ratio of wave height to water depth is ranged about 0.1–0.5 in the mouth of Pussur estuary. For Hoogly River, it is reported that the observed spring tidal range (semidiurnal) show tidal amplification over about 0–100 km and tidal damping over 100–290 km. In the Pussur River, it is found that the tidal amplification is continued up to Chalna about 90 km from mouth and after that tidal dumping occurs from Chalna to Bordia i.e. within 100–170 km. According to Prandle [35], the ratio of tidal range at 60 km upstream of a mouth of silt–mud estuary is estimated about 1.27. In this study, it is found that the tidal range during HFS in Akram Point and Mongla are 2.5 and 3.2 m, respectively (Fig. 22). Thus, the ratio of tidal range between Akram Point and Mongla is 1.28. For Hoogly River, the phase shift of HW is reported as about 1.5 h over 50 km. As shown in Fig. 22, the phase shift of HW for Pussur river is found about 1.0 h over 50 km.

For the Western Scheldt Estuary, the computed wave speed is in the range of 13–16 m/s between the mouth and station Bath at about 60 km from the mouth [36]. Van Rijn [37] reported that in amplified estuaries the real wave speed (c) is larger than the classical value [$c_o=(gh_o)^{0.5}$]. The observed wave speed in the Scheldt Estuary is about 13–16 m/s, whereas the classical value is of the order of 10 m/s. For Pussur River, considering the average depth upto Joymonirgol and Mongla as 15 and 12 m, the classical values of wave speed can be computed as 12 and 11 m/s. However, in the simulated result, the propagation speed is estimated as 14 and 13 m/s, respectively.

Based on the observation from Kapuas River, Indonesia, Kastner et al. [38] reported that along the upstream parts of the tidal river, the low depth increases the damping so that the tide more rapidly attenuates. In this study it was found that the downstream depth of the river is more than 10 m, which reduced to less than 5 m at upstream. The tidal range is found to be attenuated towards upstream and diminishes within 155–173 km upstream depending of seasonal variations. In this research, it is observed that the upstream (at Chalna) tidal range is higher in LFS (3.91 m) compared to HFS (3.75 m). Similar result is presented in a Modeling study on the Yangtze Estuary [39], and it is reported that the decrease in tides from dry to wet season is due to enhanced bottom stress generated by river-tide interactions.

5. Conclusion

The hydrodynamics of the Pussur River system is a point of interest to the researchers due to the economic and environmental importance of this river system. In this study, the hydrodynamic behavior of this river system has been simulated and the effect of discharge variation at Bordia and tidal level rise at Akram point were evaluated. Based on the simulated results following conclusions are made:

- During the dry season, the tidal effect from the sea reaches Bordia, while in the monsoon season, the tide reaches about 15 km less (up to Kalia) due to the increased flow of freshwater. Tide takes around 115 min to reach at Chalna from Akram Point and 315 min to reach at Kalia from Chalna.
- The length of the Pussur estuary is approximately 200 km, with depths ranging from 4 to 30 m. The velocity at the mouth is typically around 1 m/s. In the mouth of the Pussur estuary, the ratio of wave height to water depth typically falls between 0.1 and 0.5.

- The Pussur river experiences tidal amplification up to Chalna, located approximately 90 km from its mouth. Beyond Chalna, tidal dumping occurs upto Bordia, covering a distance of 100–170 km. The study reveals that the tidal range during HFS in Akram Point and Mongla is 2.5 and 3.2 m respectively. The tidal range ratio between Akram Point and Mongla is 1.28. The phase shift of the high water for the Pussur River is approximately 1.0 h over a distance of 50 km.
- It is observed that the upstream (at Chalna) tidal range is higher in LFS (3.91 m) compared to HFS (3.75 m). The decrease in tides from dry to wet season is due to enhanced bottom stress generated by river-tide interactions.
- Due to 50% increase of discharge in Bordia, the increase of discharges at Kalia, Chalna and Mongla were found as 43%, 7% and 2%, respectively. The difference of high-water level between Mongla and Kalia are about 1.5 m and 2.5 m for LFS and HFS, respectively. The seasonal reduction of flow is 45% and 32% in high tide and 47% and 45% in low tide at Akram point and Chalna, respectively.
- In high flow season, the velocity at Akram point is higher than Chalna, however in low flow season, the phenomena is reversed. For 0.5 m increase of water level at downstream, the high and low water level at Chalna are found to be increased by 0.15 and 0.69 m, respectively; for 1.0 m increase of water level at downstream, the high and low water level at Chalna are projected to increase by 0.67 and 1.2 m, respectively. The effect of downstream water level was found more significant in the case of low flow season.

Data availability statement

Data will be made available on request.

CRediT authorship contribution statement

Motiur Rahman: Writing – original draft, Software, Investigation, Data curation. **Md. Shahjahan Ali:** Writing – review & editing, Supervision, Methodology, Conceptualization.

Declaration of competing interest

The authors declare that they have no known competing financial interests or personal relationships that could have appeared to influence the work reported in this paper.

References

[1] E. Chávarri, A. Crave, M.P. Bonnet, A. Mejía, J. Santos Da Silva, J.L. Guyot, Hydrodynamic modelling of the Amazon River: factors of uncertainty, J. S. Am. Earth Sci. 44 (2013) 94–103, https://doi.org/10.1016/j.jsames.2012.10.010.
[2] X. Lai, J. Jiang, Q. Liang, Q. Huang, Large-scale hydrodynamic modeling of the middle Yangtze River Basin with complex river–lake interactions, J. Hydrol. 492 (2013) 228–243, https://doi.org/10.1016/j.jhydrol.2013.03.049.
[3] M. Armandei, A.C. Linhoss, R.A. Camacho, Hydrodynamic modeling of the Western Mississippi Sound using a linked model system, Reg. Stud. Marine Sci. 44 (2021, May) 101685, https://doi.org/10.1016/j.rsma.2021.101685.
[4] F.Y. Logah, A.B. Amisigo, E. Obuobie, K. Kankam-Yeboah, Floodplain hydrodynamic modelling of the lower Volta River in Ghana, J. Hydrol.: Reg. Stud. 14 (2017) 1–9, https://doi.org/10.1016/j.ejrh.2017.09.002.
[5] A.I. Pathan, P.G. Agnihotri, Application of new HEC-RAS version 5 for 1D hydrodynamic flood modeling with special reference through geospatial techniques: a case of River Purna at Navsari, Gujarat, India, Modeling Earth Syst. Environ. 7 (2) (2020) 1133–1144, https://doi.org/10.1007/s40808-020-00961-0.
[6] R.K. Singh, V.G. Kumar Villuri, S. Pasupuleti, R. Nune, Hydrodynamic modeling for identifying flood vulnerability zones in lower Damodar River of eastern India, Ain Shams Eng. J. 11 (4) (2020) 1035–1046, https://doi.org/10.1016/j.asej.2020.01.011.
[7] Z. Xue, R. He, J. Liu, J.C. Warner, Modeling transport and deposition of the Mekong River sediment, Continent. Shelf Res. 37 (2012, April) 66–78, https://doi.org/10.1016/j.csr.2012.02.010.
[8] T.V.H. Le, H.N. Nguyen, E. Wolanski, T.C. Tran, S. Haruyama, The combined impact on the flooding in Vietnam's Mekong River delta of local man-made structures, sea level rise, and dams upstream in the river catchment, Estuar. Coast Shelf Sci. 71 (1–2) (2007) 110–116, https://doi.org/10.1016/j.ecss.2006.08.021.
[9] M.Z. Rahman, U.K. Navera, Hydrodynamic scenarios to reduce the saline water intrusion in the southwest region of Bangladesh, Tech. J. 14 (10) (2016) 35–43. River Research Institute (RRI), Bangladesh, ISSN: 1606-9277.
[10] M.S. Ali, M.B. Hossen, Climate change vulnerability assessment: a case study of South west coastal community of Bangladesh, Asian J. Water Environ. Pollut. 19 (2) (2022) 25–32, https://doi.org/10.3233/AJW220020.
[11] W. Zhang, M. Rahman, H. Li, A. Ma, M.S. Ali, J. Zhang, Preliminary study on siltation in Pussur navigation channel with regulating structure, in: Book Chapter in Advances in Transdisciplinary Engineering, Volume 19: Hydraulic and Civil Engineering Technology VI, 2021, pp. 476–485, https://doi.org/10.3233/ATDE210203.
[12] M.M. Alam, Parallel lamination in sandy deposits of the Jamuna River, Bangladesh. Significance in paleo fluvial interpretation, Bangladesh Geosci. J. 2 (1996) 37–46.
[13] A.R.M.T. Islam, Assessment of fluvial channel dynamics of Padma River in northwestern Bangladesh, Univ. J. Geosci. 4 (2) (2016) 41–49, https://doi.org/10.13189/ujg.2016.040204.
[14] A. Aziz, A. Paul, Bangladesh sundarbans: present status of the environment and biota, Diversity 7 (3) (2015) 242–269, https://doi.org/10.3390/d7030242.
[15] A. Zaman, M. Molla, I. Pervin, S.M. Rahman, A. Haider, F. Ludwig, W. Franssen, Impacts on river systems under 2 °C warming: Bangladesh Case Study, Clim. Serv. 7 (2017) 96–114, https://doi.org/10.1016/j.cliser.2016.10.002.
[16] R.L. Bain, R.P. Hale, S.L. Goodbred, Flow reorganization in an anthropogenically modified tidal channel network: an example from the southwestern Ganges-Brahmaputra-Meghna Delta, J. Geophys. Res. Earth Surf. 124 (2019) 2141–2159, https://doi.org/10.1029/2018JF004996.
[17] IWM, Feasibility Study for Improvement of Navigability of Mongla Port, Mongla Port Authority, Mongla, Bagerhat, Bangladesh, 2004.
[18] M. Rahman, M.S. Ali, Morphological response of the Pussur River, Bangladesh to modern-day dredging: implications for navigability, J. Asian Earth Sci. X 7 (2022) 100088, 10.1016/j.jaesx.2022.100088. 36.
[19] D. van Maren, J. Beemster, Z. Wang, Z. Khan, R. Schrijvershof, A. Hoitink, Tidal amplification and river capture in response to land reclamation in the Ganges-Brahmaputra delta, Catena 220 (2023) 106651, https://doi.org/10.1016/j.catena.2022.106651.
[20] M.M. Rahman, M.S. Ali, Hydrological Characteristics of Pussur River and its Navigability. Proceedings of the 4th International Conference on Civil Engineering for Sustainable Development (ICCESD-2018), 7~9 Feb., KUET, Bangladesh, 2018, 5091-1–5097-11, http://iccesd.com/proc_2018/Papers/r_p5097.pdf.

[21] T. Tingsanchali, M.F. Karim, Flood hazard and risk analysis in the southwest region of Bangladesh, Hydrol. Process. 19 (10) (2005) 2055–2069, https://doi.org/10.1002/hyp.5666.
[22] M.S. Ali, T. Mahzabin, T. Hosoda, Impact of climate change on floods of Bangladesh and introducing flood intensity index to characterize the flooding scenario, J. Eng. Sci. 4 (1) (2013) 23–34.
[23] J. Pethick, J.D. Orford, Rapid rise in effective sea-level in southwest Bangladesh: its causes and contemporary rates, Global Planet. Change 111 (2013) 237–245, https://doi.org/10.1016/j.gloplacha.2013.09.019.
[24] M.S. Ali, K. Syfullah, Effect of sea level rise induced permanent inundation on the livelihood of polder enclosed beel communities in Bangladesh: peoples' perception, J. Water Clim. Change, IWA 8 (2) (2017) 219–234, https://doi.org/10.2166/wcc.2016.236.
[25] M.S. Horritt, G. Di Baldassarre, P.D. Bates, A. Brath, Comparing the performance of a 2D finite element and a 2D finite volume model of floodplain inundation using airborne SAR imagery, Hydrol. Process. 21 (2007) 2745–2759.
[26] M.S. Ali, Model Refinement of Unsteady RANS and its Practical Applications in the Field of Hydraulic Engineering, PhD Thesis, Kyoto University, Japan, 2008, https://doi.org/10.14989/doctor.k14139.
[27] K.D.W. Nandalal, Use of a hydrodynamic model to forecast floods of Kalu River in Sri Lanka, J. Flood Risk Manage. 2 (2009) 151–158.
[28] M.S. Ali, T. Hosoda, I. Kimura, Unsteady RANS computation of compound channel flows with large scale vortices and secondary currents, in: Proceedings of 5th International Symposium on Environmental Hydraulics, Tempe, Arizona, USA, 2007. http://www.iahr.net/e-shop/store.
[29] W. Majewski, Urban flash flood in Gdańsk-2001; solution and measures for city flood management, Int. J. River Basin Manag. (2008) 357–367.
[30] N. Pramanik, R. Panda, D. Sen, One-dimensional hydrodynamic modeling of river flow using DEM extracted river cross-section, Water Resour. Manag. 25 (2009) 835–852.
[31] M. Horritt, P. Bates, Evaluation of 1D and 2D numerical models for predicting river flood inundation, J. Hydrol. 268 (1–4) (2002) 87–99, https://doi.org/10.1016/s0022-1694(02)00121-x.
[32] M.M. Rahman, M.S. Ali, Potential causes of navigation problem in Pussur River and interventions for navigation enhancement, in: Proceedings of the 4th International Conference on Civil Engineering for Sustainable Development (ICCESD-2018), 7~9 Feb., KUET, Bangladesh, 2018, 5100-01 to 5100-15, http://iccesd.com/proc_2018/Papers/r_p5100.pdf.
[33] M.S. Ali, M.M. Hasan, Environmental flow assessment of Gorai River in Bangladesh: a comparative analysis of different hydrological methods, Heliyon 8 (7) (2022) e09857, https://doi.org/10.1016/j.heliyon.2022.e09857. Elsevier Ltd.
[34] M. Soeb, M.S. Ali, S.M. Hassan, Simulation of sidr-like cyclone using mri storm surge model with various initial strength: a Bay of bengal context, in: American Institute of Physics (AIP) Conference Series, vol. 2713, AIP Publishing, 2023 050010, https://doi.org/10.1063/5.0129836, 1.
[35] D. Prandle, How tides and river flows determine estuarine bathymetries, Prog. Oceanogr. 61 (2003) 1–26.
[36] H.H.G. Savenije, Salinity and Tides in Alluvial Estuaries, Elsevier, New York, 2005.
[37] L.C. van Rijn, Analytical and numerical analysis of tides and salinities in estuaries; part I: tidal wave propagation in convergent estuaries, Ocean Dynam. 61 (2011) 1719–1741, https://doi.org/10.1007/s10236-011-0453-0.
[38] K. Kästner, A.J.F. Hoitink, P.J.J.F. Torfs, E. Deleersnijder, N.S. Ningsih, Propagation of tides along a river with a sloping bed, J. Fluid Mech. 872 (2019) 39–73, https://doi.org/10.1017/jfm.2019.331.
[39] N.C. Alebregtse, H.E. de Swart, Effect of river discharge and geometry on tides and net water transport in an estuarine network, an idealized model applied to the Yangtze Estuary, Continent. Shelf Res. 123 (2016) 29–49, https://doi.org/10.1016/j.csr.2016.03.028.